Materials Today Communications 13 (2017) 359–366

Contents lists available at ScienceDirect

Materials Today Communications

journal homepage: www.elsevier.com/locate/mtcomm

Temperature dependence of dynamic and mechanical properties in poly (acrylic acid)/graphene oxide nanocomposites

Georgios Kritikos*, Kostas Karatasos

Laboratory of Physical Chemistry, Department of Chemical Engineering, Aristotle University of Thessaloniki, 54124, Thessaloniki, Greece

ARTICLE INFO

Keywords:
Equation of state
Molecular dynamics
Glass transition
Poly(acrylic acid)
Graphene oxide
Nanocomposites

ABSTRACT

In this work we present a novel methodology with the use of which a new Equation of State (EoS) combined with molecular dynamics (MD) simulations may allow an accurate extrapolation of the dynamic and mechanical properties of polymer nanocomposites in the glassy region. By fitting the temperature dependence of the specific volume to the EoS, the super-Arrhenius increase in the activation energy can be determined. Based on a sigmoidal function of the activation energy, a VFT-like equation is derived which incorporates a new parameter (δ_g) that determines the extent of the super-Arrhenius region. The new equation identifies two components for the diffusion immediately above and below the glass transition temperature, T_g. Application of the proposed methodology is demonstrated in Poly(acrylic acid) (PAA)/Graphene oxide (GO) nanocomposite systems. A shift of T_g at higher temperatures is predicted due to the addition of GO. Based on the temperature dependence of the viscosity, it is shown that the increase in T_g leads to improved mechanical properties in the composites. In case of an increase in δ_g at constant T_g, the ratio of the shear modulus of the nanocomposite over the shear modulus of the bulk shows an enhancement consistent with the well-known "Payne effect".

1. Introduction

Insertion of nanoparticles into a polymer matrix is a common practice in order to enhance polymer performance [1]. The enhancement of several physical properties (including the mechanical behavior) in such composite materials, has been found to correlate with the modification of the glass transition temperature with respect to that of the pristine polymer [2–4]. Therefore, the ability to predict the glass behavior of polymer composites is of paramount importance, for the design, the optimization of the processing conditions and ultimately for the improvement of the physical behavior of these materials [5]. To this end, a significant effort has recently be devoted in order to understand the elementary mechanisms which are responsible for the manifestation of glass transition phenomena in polymer-based composite materials [4,6–8].

Among the systems studied in recent years, special focus has been placed on graphene-based polymer composites [9–11] due to the exceptional properties related to mechanical, thermal, electronic and gas-barrier properties of graphene (see refs [12,13] and references therein). More specifically, combination of graphene-based fillers with polar polymeric matrices may lead to the fabrication of composite materials which can be utilized in high added value applications, such as in fuel cell membranes [14,15], in responsive systems for water clean-up [16] and in chemical [17] and biological sensors [18]. Polar polymers appear to intermix more effectively with a functionalized form of graphene, graphene oxide (GO) [19–21]. Polymer/GO nanocomposites have presented high ion-exchange capacity, phosphate adsorption ability, electron transfer number in the oxygen reduction process, electrochemical luminescence activity and good solubility and stability [22].

The unique structure and high surface area of GO facilitates a higher degree of proton transport improving conductivity and mechanical properties of the composites [23]. Ion conductivity in such polar-polymer/GO membranes [24] is determined by the diffusion properties near the glass transition temperature (T_g). Viscosity and diffusion coefficients are not governed by an Arrhenius equation of constant activation energy but by a super-Arrhenius behavior [8,25–27]. The temperature dependence of the diffusion is qualitatively described by the Vogel-Fulcher-Tammann (VFT) equation [28–30], which nevertheless does not take into account the extension of the super-Arrhenius region. In other words, it does not include any parameter referring to a critical crossover temperature well above T_g [25,32,33]. Particularly in polymer/graphene nanocomposites, it is not as yet clear through which mechanisms polymer properties are enhanced [4,34–37]. Therefore, any model capable of predicting the dynamic and mechanical characteristics of such nanocomposites would have to deal with the complex

* Corresponding author.
E-mail addresses: kritikgio@gmail.com, kritikgio@cheng.auth.gr (G. Kritikos).

https://doi.org/10.1016/j.mtcomm.2017.11.006
Received 27 October 2017; Received in revised form 7 November 2017; Accepted 7 November 2017
Available online 08 November 2017

glassy dynamics of macromolecules near the polymer/filler interface and/or under confined conditions.

Computer simulations have been proven a valuable tool in the study of molecular dynamics at the atomistic level [15,27,32,38–41]. Both Molecular Dynamics (MD) and Monte Carlo (MC) simulations [40,42] have been utilized extensively for the clarification of interfacial polymer/filler dynamics. Nevertheless, under the dominant kinetic interpretation [33] of the glass transition the predictions of the molecular simulations at the glassy region are approached with skepticism. Although the specific volume temperature dependence obtained by MD indicates one T_g, it is in general accepted that the properties of polymers in the glassy region (in bulk or confinement conditions) should not be described by an Equation of State (EoS) or a single T_g [25,33,43]. On the other hand, a combined methodology based on molecular simulations and on an EoS proved particularly effective [8,44], attesting to the potential of the description of thermodynamic properties and local dynamics even in the vicinity of the glass transition region. It may thus provide an additional path for the interpretation of glass transition phenomenology beyond the currently prevailing models, emphasizing also the thermodynamic aspect of glass-related phenomena.

Despite the great technological potential of the aforementioned composite systems, to our knowledge, only few [15,44–47] computational studies have as yet addressed issues concerning dynamic, structural and mechanical properties in the fully atomistic level, in dispersions of polar polymers enriched with carbon-based fillers such as GO. In this work, we will present results for PAA/GO nanocomposites representing melt-mixed systems, obtained by means of MD simulations. The simulation results will be described via an equation of state that will enable the determination of the temperature dependence of the activation energy of local polymer dynamics. Insertion of the so-obtained activation energy to a new VFT-like equation will allow extrapolation of the dynamic properties determined by MD simulations, to the glassy region which involves long relaxation times. We will also discuss the influence of the degree of confinement of PAA in the mechanical properties of the examined composites by examining two different GO loadings.

2. Model description and simulation protocol

For the purposes of our study we have simulated three systems. One pristine polymer system consisting of 40 PAA atactic chains with 40 monomers each and two nanocomposites comprised by 30 PAA chains identical to those of the pristine system, mixed either with 7 or with 18 GO flakes. The examined systems will be referred to as 40PAA40, 30PAA7GO and 30PAA18GO respectively. The average radius of gyration of the PAA chains consisting of 40 monomers (MW = 2884.52 g/mol, below the entanglement MW) was estimated from our simulations to be approximately 14 Å. The dimensions of the GO flakes were 15 Å × 20 Å and resulted in composite systems of 14.5 wt% and 30.3 wt% in GO for the 30PAA7GO and 30PAA18GO respectively. We have opted for GO flakes bearing a size comparable to the average dimensions of the polymer chain in order to facilitate a good intermixing of the two components and thus an increased interfacial area between the polymer chains and the GO nanosheets. The graphene-oxide flakes were modelled (Fig. S1 in the Supplementary material) with a carbon to oxygen atom ratio of 5:1 and a hydroxyl to epoxy group ratio of 3:2 approximately [44]. We have described the PAA/GO system based on the AMBER forcefield [48]. The Gasteiger method was used for charge assignment on PAA chain [49], while the partial charges for the carbon and oxygen atoms of GO were taken from ref [50].

The initial system configurations were obtained by mixing molecules with the use of the Packmol program [51]. In order to obtain well equilibrated structures (Fig. S2 in the Supplementary material) we have used the protocol described in previous works [44,52] which involves an annealing procedure in conjunction with energy minimization and MD runs. Namely, at each temperature energy minimization is followed by MD simulations lasting several hundreds of ns (depending on the temperature) in the isobaric-isothermal ensemble (NPT), under periodic boundary conditions at 1 atm pressure. For the generation of the long simulation trajectories at each temperature we have utilized the NAMD 2.11 software [53]. For the part of the study involving deformation we have also employed the LAMMPS package [54]. In the equilibrated conformations, we have implemented an axial deformation of constant strain rate of $1.0 \times 10^8\ s^{-1}$, while in the other two dimensions a Berendsen barostat [54] was used in equilibrium keeping the external pressure at 1 atm. The thermostat was the same with the one chosen in the NAMD simulations [44] while the transverse box dimensions were coupled.

3. Results and discussion

3.1. Fitting to EoS

The original lattice fluid model [55–57] allows an efficient calculation of the entropy in macromolecular systems while by incorporating a mean field approach for the interaction energy leads to an accurate EoS at the region of constant activation energy. In order to introduce the structural heterogeneities that are present in the glassy region, we have proposed a modification of the mean field [8]. Assuming that during the glass transition the material does not undergo a first order transition, then the system should obtain gradually a fraction (f) of the energy step from the liquid state of interaction energy T_2^* to solid state of interaction energy T_1^*. Moreover, the entire transition can be considered to take place in a temperature interval δ_g within which the pairwise interaction energy T^* can be described as:

$$T^* = T_2^* + \frac{1}{1 + exp\left(\frac{T - T_g}{\delta_g}\right)}(T_1^* - T_2^*) \tag{1}$$

where the factor $f = 1/\left(1 + exp\left(\frac{T - T_g}{\delta_g}\right)\right)$ represents a sigmoidal switching function of temperature, T_g denotes the glass transition temperature and δ_g defines the extent of the super-Arrhenius region [8].

By inserting a sigmodal function (Eq. (1)) for the pairwise energy (attractive interaction energy between adjacent segments) to a simple lattice EoS [55], a new equation is derived, which provides a description of the Solid to Liquid Glass (SLG) transition. We will refer to the new EoS [8] henceforth, as SLG:

$$\frac{P v^*}{RT} + \left(1 - \frac{1}{r}\right)\left(\frac{\rho}{\rho_o}\right) + ln\left(1 - \frac{\rho}{\rho_o}\right) + \left(\frac{T_2^*}{T} + \frac{T_1^* - T_2^*}{T\left(1 + exp\left(\frac{T - T_g}{\delta_g}\right)\right)}\right)\left(\frac{\rho}{\rho_o}\right)^2 = 0 \tag{2}$$

In Eq. (2), ρ_o is the density at zero free volume (close to the Vogel temperature [28], T_{Vog}), v^* is the segmental volume on the lattice, r is the number of segments in a chain that represents the macromolecule and T_2^*, T_1^* are the characteristic pairwise energies divided by the Boltzmann's constant (ε^*/k) [55], at the Arrhenius region and at the solid state respectively [8]. A similar function for the pairwise parameter (T^*) was also proposed by earlier computational studies on unequal-sized hard sphere systems [33] that can simulate glass transition. Since the interpretation of the observed transition was kinetic, it was not accompanied by any thermodynamic explanation of the temperature dependence of the interaction energy. In the present work we will try to shed light on what kind of cooperative dynamics a sigmoidal pairwise energy is related to. In a forthcoming study we intend to elaborate more on the universality of the proposed model.

Fig. 1 presents the temperature dependence of the specific volume from 350 K to 650 K, for all the examined systems.

One of the key results of the present work is that the simulation data

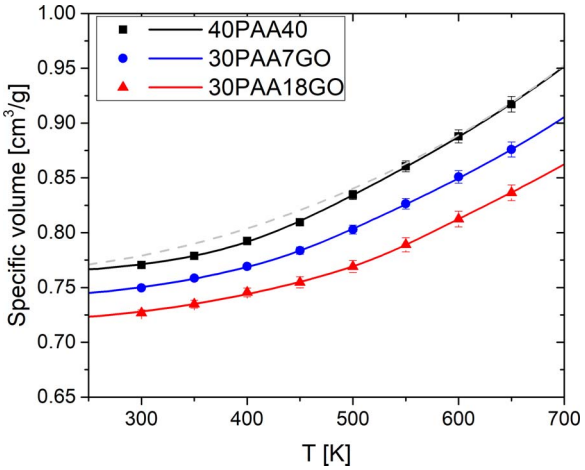

Fig. 1. Temperature dependence of the specific volume for the bulk (40PAA40, black) the nanocomposite with 7 GO flakes (30PAA7GO, blue) and the nanocomposite with 18 GO flakes (30PAA18GO, red). The fitting was performed using the SLG (see text, Eq. (2)), while we present with a dashed light grey line the prediction of the original Sanchez-Lacombe EoS [55] for the 40PAA40.

of the specific volume for various concentrations in nanofillers can be fitted reliably by the SLG equation [8] which requires a rather small number of adjustable parameters. For the case of the 40PAA40 system we also show the fitting with the original lattice fluid EoS [55] where the pairwise energy was set constant and equal to T_2^*. It is clear that a temperature independent interaction energy fails to describe the density at the glassy region. As demonstrated in previous works [8,44] the SLG equation shows an excellent agreement with classical force fields describing non-polar polymers such as polyethylene but also with polar polyelectrolytes like PAA, where an extended degree of hydrogen-bonding is present [44].

Fitting the temperature dependence of the specific volume to the SLG, resulted in T_g values of 412 ± 5 K, 450 ± 10 K and 530 ± 10 K and in δ_g parameters of 45 ± 3 K, 40 ± 6 K and 34 ± 8 K, for the 40PAA40, 30PAA7GO and 30PAA18GO systems, respectively. The constant v^* which characterizes the size of the lattice site was determined by a fitting to the specific volume values of the bulk system (Fig. 1 squares), to be equal to 54.8 cm^3/mol; this parameter was kept constant when fitting the analogous behavior of the composite systems as well. In all three systems, we have assumed a constant pressure (P) of 1 atm and different values of ρ_o equal to 1.31 g/cm^3, 1.35 g/cm^3 and 1.39 g/cm^3, resulting [55] to different values of r, amounting to 40, 39 and 38 for the 40PAA40, 30PAA7GO and 30PAA18GO systems, respectively. Values of the T_2^* parameter were estimated at 908 K, 945 K and 987 K, while those of T_1^* at 1100 K, 1022 K and 1048 K for 40PAA40, 30PAA7GO and 30PAA18GO respectively.

The value of the glass transition temperature as estimated by means of Eq. (2), was found to be consistent with the results of the method relying on the change in the slope of the specific volume [39]. For the case of bulk PAA it was also checked by comparing to available experimental results with the use of Modulated DSC [58] that indicated a T_g equal to 401 K. According to our model which is based on thermodynamic arguments, the calorimetric T_g is influenced by the cooling rate since the heat capacity step is affected by the cooling rate.

The divergence of the T^* from the constant value (T_2^*) [55] is rationalized by the structural heterogeneity that originates from the entropic force [8,27,59] for diffusion in areas where a cage is formed. We are referring to a dynamic situation related to the formation of cooperative rearranging regions (CRRs) [27,60]. The density fluctuations are schematically described in Fig. 2. A fraction of dense regions with a T^* close to T_1^* (colored blue) could allow diffusion in regions with a T^* close to T_2^* (colored white). Assuming that the fraction of the regions with T_2^* is α_2, then $T^* = \alpha_2 T_2^* + (1-\alpha_2) T_1^*$. This is a new idea of a

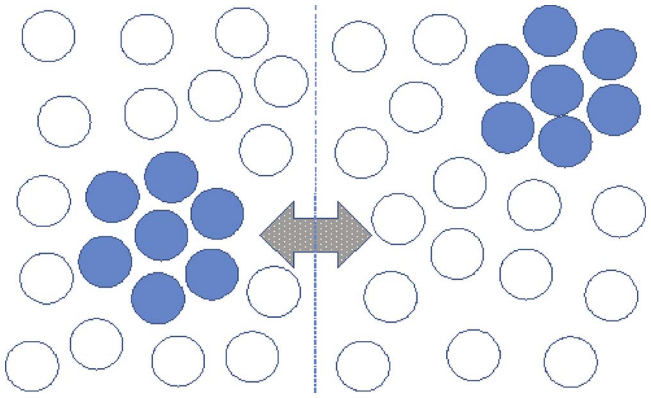

Fig. 2. Structural heterogeneities above T_g. The dynamic nature of the CRRs is depicted by the two-directional arrow.

varying mean field and it was introduced [8] in order to explain the super-Arrhenius region, based on a previous approach [61] for the introduction of structural heterogeneities on the lattice [57]. Since at high temperatures [25], where $\alpha_2 = 1$, the relaxation follows an Arrhenius behavior of constant activation temperature A (activation energy/k), we may assume that at the super-Arrhenius region the activation temperature will take a value equal to $A\frac{T_1^* - T_2^*}{T_1^* - T^*}$. The T_g value estimated via fitting to the SLG equation is defined as the temperature where the T^* is equal to the value at half the step from T_1^* to T_2^*.

In Fig. 3 we present the distribution of the difference between the local molecular volume and the mean molecular volume, for the 40PAA40 system at various temperatures. As local molecular volume we define the summation of atomic volumes calculated via a Voronoi tessellation of space [54], while the mean molecular volume is taken as the volume of the simulation box divided by the number of molecules. It is reasonable to assume that in the white regions of Fig. 2, the molecular volume is described by a normal distribution that is disrupted by a small fraction of high density, blue regions. Based on the divergence of T^* from T_2^* at temperatures above T_g in the super Arrhenius region, an anomaly in the molecular volume distribution might have been anticipated. However, only small deviations from the normal distribution at high temperatures (Fig. 3) are observed. This could be related to the size of the simulation box (size effect); a simulation box with dimensions approximately 4 times the R_g of the polymer chains, as was the case in our simulations, might have somewhat affected the extent of the

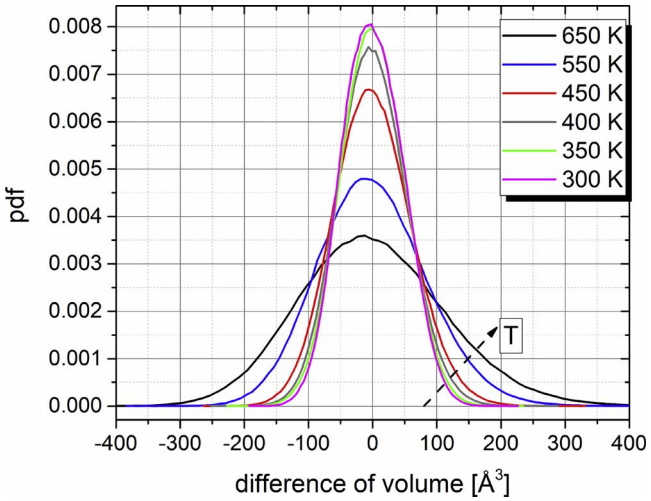

Fig. 3. Probability distribution function (pdf) of the difference of the molecular volume from the mean molecular volume, for the 40PAA40 system, at various temperatures. The negative values correspond to molecular conformations of lower than the average volume, while the opposite stands for the positive values.

observed heterogeneities [27,39]. At T_g and temperatures below, a normal distribution characterizes the molecular volumes. Replication at T_g of the heterogeneities through the periodic boundary conditions is not expected to affect the shape of the real molecular volume distribution, which has a cumulative function of sigmoidal characteristics. Nevertheless, it may affect the aging kinetics below T_g. Experimentally, aging evolves through relaxation of regions of low density which propagates to regions of high density towards uniform density, in a process realized at macroscopic timescales [25]. In simulations, density relaxation in the elementary box is replicated to all its periodic images (i.e., spanning simultaneously the entire equivalent macroscopic system) leading thus to an effective accelerated aging.

3.2. Dynamic properties

The super-Arrhenius increase in the activation energy as determined by the fitting of the density's temperature dependence, can be inserted in an Arrhenius equation in order to describe glassy dynamics. The resulted equation associated with the timescale of α-relaxation, therefore, takes the following form:

$$\tau = \tau_o \exp\left(\frac{A}{T}\left[\frac{T_1^* - T_2^*}{T_1^* - T^*}\right]\right) \quad (3a)$$

where A represents the activation temperature at the Arrhenius region and $\tau_\circ$ is a constant with units of time. Eq. (3a) is a VFT-like equation where in place of the difference from the Vogel temperature, now the difference between T^* and $T_1{}^*$ normalized by the step $T_1{}^*$-$T_2{}^*$, appears instead. By substituting the sigmoidal function of the pairwise parameter (Eq. (1)) to the Eq. (3a) we obtain:

$$\tau = \tau_o \exp\left(\frac{A}{T}\left[\exp\left(\frac{T_g - T}{\delta_g}\right) + 1\right]\right) \quad (3b)$$

We will call the new VFT-like equation "KK" (Kritikos-Karatasos).

In Eq. (3b), we can identify two components of the diffusion in the glassy region. A non-Arrhenius and an Arrhenius part acting simultaneously. We may assume that the cooperative diffusion is allowed at temperatures just above T_g where each component of the diffusion requires an activation energy no higher than A. At temperatures just below T_g, diffusion is suppressed; the material is trapped in liquid conformations, it exhibits a heat capacity step and it undergoes glass transition. This is followed by a relaxation/aging procedure towards structural homogeneity/energy minimized configurations. As the cooperative diffusion is obstructed at temperatures below T_g, this is manifested as a change in the slope of the specific volume. According to experimental findings below T_g, only Arrhenius-like dynamics is observed, usually ascribed to β-relaxation [25]. The Arrhenius part above T_g has been also confirmed experimentally under conditions of extreme confinement [27,62–64].

Fig. 4 shows the relaxation times of the autocorrelation function of the unit vectors ($\vec{e}$) of the backbone bonds of PAA, which can be associated with α-relaxation [25]. The orientational correlation function was represented by a second order Legendre polynomial of the form:

$$P_2(t) = 0.5[3\langle[\vec{e}(t)\cdot\vec{e}(0)]^2\rangle - 1] \quad (4)$$

To fit the so-calculated spectra we employed the mKWW function [25] given by:

$$P(t) = \alpha_{lib}\exp\left[-\frac{t}{\tau_{lib}}\right] + (1-\alpha_{lib})\exp\left[-\left(\frac{t}{\tau_{seg}}\right)^{\beta}\right] \quad (5)$$

Parameter α_{lib} can be interpreted as the fraction of regions with Debye relaxation while the β parameter (stretched exponent) accounts for the contribution of similar relaxation processes arising from a distribution of local environments. The relaxation time in regions where the molecule diffuses freely is described by the τ_{lib} while the relaxation at the segmental scale is described by τ_{seg}. The overall decorrelation time τ_c is then taken as a weighted average of the form $\tau_c = \alpha_{lib}\tau_{lib} + (1-\alpha_{lib})\tau_{seg}\frac{1}{\beta}\Gamma\left(\frac{1}{\beta}\right)$ (Γ stands for the Gamma function) and is illustrated in Fig. 4. Fitting of the relevant simulation data with Eq. (3b) by using fixed T_g and δ_g values (as calculated via the temperature dependence of the specific volume) led to the determination of activation temperatures, A, of 4836 K, 3074 K and 740 K and $\tau_\circ$ parameters of 7.5×10^{-3} ns, 0.2 ns and 23.1 ns for the 40PAA40, 30PAA7GO and 30PAA18GO systems, respectively.

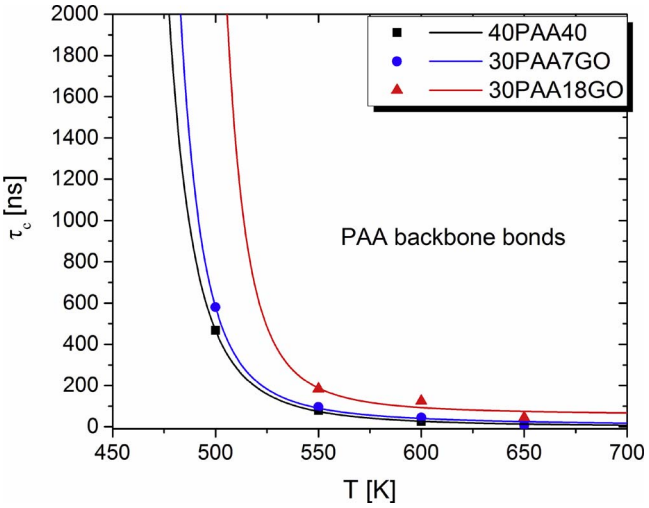

Fig. 4. Temperature dependence of orientational relaxation times of the backbone carbon bonds (C—C) of PAA at the pristine system, 40PAA40 and the two nanocomposites, 30PAA7GO and 30PAA18GO.

An analogous agreement in the description of the temperature dependence of the decorrelation times defined by Eq. (3b) was also verified (see Fig. S3 in supported information) for the second order correlation function of the unit vectors connecting the center of mass of a polymer chain with its atoms, describing the overall chain reorientation [44]. In this case, for the estimation of the decorrelation times and in order to include lower temperatures as well, a shifting procedure was performed based on the time–temperature superposition principle, as described in ref [44]. Parameters A were estimated to be 3310 K, 1615 K and 703 K, while the corresponding $\tau_\circ$ values were estimated at 0.1 ns, 10 ns and 119 ns for the 40PAA40, 30PAA7GO and 30PAA18GO models, respectively.

In order to check the applicability of the proposed methodology for the estimation of T_g, we have used Eq. (3b) to fit the dielectric results for poly(styrene) (PS) as published by Schönhals et al. [65]. The comparison is shown in Fig. S4 (in the Supplementary material) and the fitting parameters are: $T_g = 367 \pm 2$ K, $\delta_g = 20 \pm 5$ K, $A = 7294 \pm 20$ K and $\tau_\circ = 2.86 \pm 0.1$ fs. The values of the calculated T_g and A are very close to the ones presented in the experimental study on PS, given as: 373 K and 8239 K respectively [65]. Moreover, the calculated T_g through Eq. (3b) agrees with the calorimetric (Differential Scanning Calorimetry, DSC) evaluation of T_g and it is the only T_g according to the SLG equation.

3.3. Mechanical properties

Fig. 5 presents the stress-strain curves of the three systems at 350 K. The slope in the linear region of the curves resulted in values of the elastic modulus of 4.4 ± 0.2, 4.6 ± 0.2 and 5.3 ± 0.2 GPa for 40PAA40, 30PAA7GO and 30PAA18GO, respectively. We note that in order to reduce the noise of the stress-strain curves from the MD simulations we have applied a the Savitzky-Golay signal processing method, with points of window equal to 500 and of polynomial order 2.

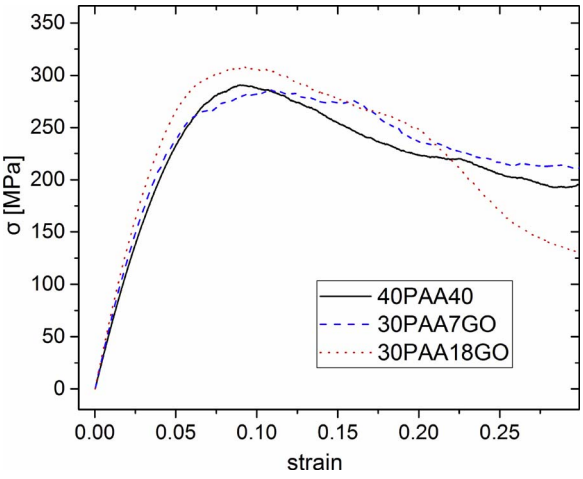

Fig. 5. Stress-strain curves for the bulk and the two nanocomposite systems at 350 K.

Moreover, it must be taken into account that the cooling rate might affect the absolute values but not the relative behavior of the calculated curves [66]. Inclusion of the GO nanoflakes (which imparts an increase in the T_g as described earlier) essentially propagates the heterogeneities/super-Arrhenius behavior to higher temperatures, increasing thus the viscosity and leading to an enhancement of the mechanical properties [66–68]. As demonstrated in our previous work [44], the slowed down local dynamics of the PAA in the nanocomposite systems is mainly attributed to the adsorbed layer, a few Å thick, adjacent to the GO flakes.

Fig. 6 depicts the PAA stresses recorded during the deformation, for the adsorbed layer (0–4 Å from the surface) and the second layer (4–8 Å from the surface). As anticipated, the adsorbed layer bearing an increased density with respect to the bulk, is characterized by negative stresses [27]. This layer retains the negative stresses even during the imposed strain. The opposite behavior is observed for the second layer. The positive stresses of the layer next to the adsorbed one is present in both, the 30PAA7GO and the 30PAA18GO systems, although in the latter model the average inter-flake distance becomes shorter, affecting probably the statistics. The resistance to deformation seems to originate from the second layer, but this is triggered by the negative stresses of the adsorbed layer. Moreover, a positive contribution to the total stresses was also confirmed from the GO during the elongation

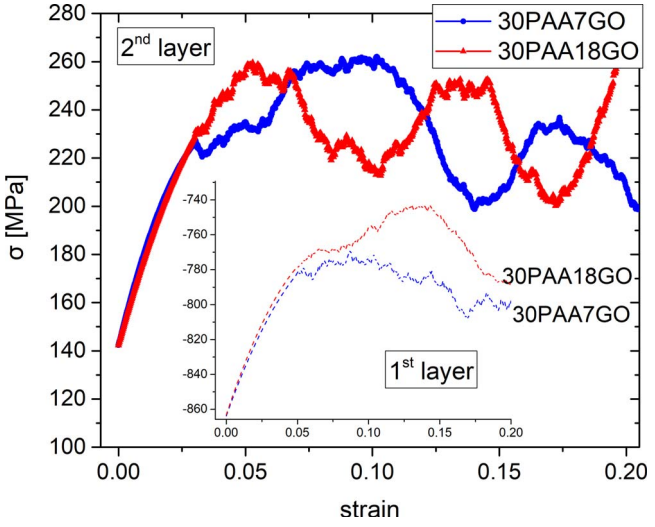

Fig. 6. Stress-strain curves of only the PAA at the two first layers of width equal to 4 Å from the GO plane for the two nanocomposite systems. The *x*,*y*-axes of the inset (1st layer) have the same units with the main graph (2nd layer).

experiment. We note that the temperature of 350 K is below the estimated T_g in both nanocomposite systems. Nevertheless, the deformation (negative pressure) should cause a change in the free volume and may result to density values characteristic of higher temperatures.

Based on an equation that describes the temperature dependence of dynamic properties, we can proceed to make predictions regarding the viscosity and also to extrapolate mechanical properties in a wider temperature range. For the shear modulus, the following relation can be derived through the viscosity [69]:

$$G = \frac{G_{ref}}{\exp\left(\frac{A}{T_{ref}}\left[\exp\left(\frac{T_g - T_{ref}}{\delta_g}\right) + 1\right]\right)} \exp\left(\frac{A}{T}\left[\exp\left(\frac{T_g - T}{\delta_g}\right) + 1\right]\right) \quad (6)$$

We have taken 400 K as a reference temperature (T_{ref}) for 40PAA40, almost 10 K below the computationally determined T_g. The value of the G_{ref} at this temperature was estimated to be approximately 1 GPa. Since MD predicts a linear temperature dependence of the modulus below T_g [66], we have considered for the two nanocomposite systems a reference temperature that resides also 10 K below their respective T_g and the same shear modulus reference value of 1 GPa. The activation temperatures, A, were set equal to the values estimated by the fitting to the backbone bond decorrelation times (Fig. 4). The results for all three systems are shown in Fig. 7. Evidently, the increase in T_g is translated to an improvement in the mechanical properties in a broad temperature range.

In past studies it has been demonstrated [7,8,63,70] that an enhancement of mechanical properties can be also accompanied by a reduction/stabilization of the characteristic glass transition temperature and heat capacity steps, as observed in calorimetric experiments. In such cases an Arrhenius-like behavior was noted [7,8,63]. In previous works it was also argued [8] that in case of extreme confinement [8,71,72], the entropic force for diffusion may cause a gradual immobilization of the adsorbed/bound layer; thus a decoupling between the mobile and the rigid amorphous phases may provide a stable, static liquid path of Arrhenius behavior [27]. In such instances a reduction of the estimated T_{Vog} was recorded [63]. To explore this effect in the framework of the proposed model and in order to elaborate more on the significance of parameter δ_g that describes the super-Arrhenius region, we have investigated for the bulk system (40PAA40) the influence of δ_g on the shear modulus. To do so, we have calculated the ratio (R) of the shear modulus at different values of δ_g over the shear modulus at the original δ_g value, while keeping constant the T_g. The results are shown in Fig. 8. It is demonstrated that the extension of the Arrhenius region may also result in an enhancement of the modulus, a few degrees above

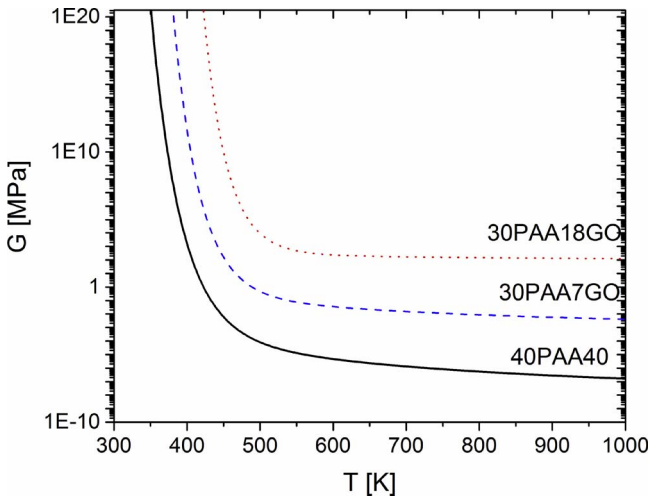

Fig. 7. Temperature dependence of the shear modulus (G) as described by Eq. (6) for the bulk, 40PAA40 system and the two nanocomposite systems 30PAA7GO and 30PAA18GO.

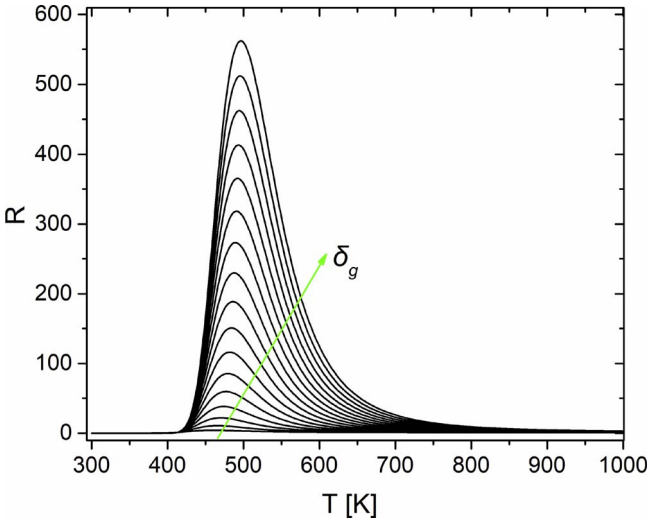

Fig. 8. Ratio ($R \equiv G/G_o$) of the shear modulus (G) of the bulk system at various values of δ_g from 65 to 385 K with a step of 20 K divided with the shear modulus value (G_o) for the original δ_{go} value, equal to 45 K.

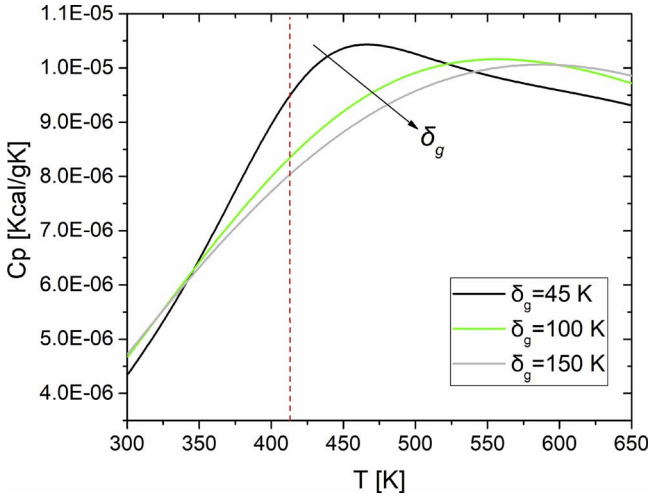

Fig. 9. Heat capacity step for the bulk system for three different values of δ_g. Only the pairwise energy contributions, as predicted by the SLG equation, were taken into account. The vertical red dash line denotes the T_g.

T_g. The temperature at which R assumes its maximum increases from 454 K at δ_g = 46 K to 498 K at δ_g = 385 K. The derivative of the increase in the peak value of R with respect to δ_g shows a maximum at δ_g = 367 K. Considering that results from computer simulations [8,27] indicate that the enhancement in the mechanical properties is observed when the interparticle distance ($h = d_{np}[(\Phi/0.74)^{-1/3}\text{-}1]$) [73] becomes comparable to the dimensions of the molecule ($h \sim R_g$), we may assume that the value of δ_g = 367 K should be related to a percentage in filler particles (Φ) close to 30 vol%, for spherical nanoparticles [63] with dimensions three times the size of the polymer molecule ($d_{np} \cong 3\,h$). We are referring to well dispersed in the polymer matrix nanofillers. Our structural analysis in the examined models showed a random dispersion of individual GO flakes or of oligomeric (2–3 flakes) clusters (see ref [44] and Fig. S2 in the supplementary material). Moreover, assuming that the T_{Vog} can be approximated by a value close to 50 K below T_g [60], then based on the free volume/density behavior, T_{Vog} drops from 362 K at δ_g = 45 K to 348 K at δ_g = 367 K. Although, the results for the shear modulus ratio (R) could be improved by a more accurate relationship between shear modulus and viscosity, it is worth noticing that the observed behavior is consistent with the reinforcement mechanism in polymer nanocomposites [4]. Since deformation in such systems affects the inter-particle distance, it could give rise to dynamic structural heterogeneities that are related to reduced δ_g values; this in turn could result in a decrease in the total stresses [27] and thus affect the modulus. On these grounds, the results of the analysis presented here provide new insight into the mechanism that is related to the "Payne effect" [4,74].

In case of extreme confinement above T_g, where a spatial isolation of the Arrhenius component of the diffusion may take place [7,8,62,63], the non-Arrhenius part of Eq. (3b) should essentially describe the average dynamics of the bound layer. In consistency with previous computational works [8], the transition of the bound layer is estimated to be stronger (larger δ_g) compared to the bulk glass transition. Moreover, the absence of a trace for the immobilization of the significant fraction of the bound layer in polymer nanocomposites, in a typical DSC thermogram, supports the idea of a large δ_g [8]. Fig. 9 plots the heat capacity as calculated by the intermolecular energy contribution using the SLG equation [8]. We note that the curves refer to the average heat capacity of the entire system. In contrast, in a typical DSC experiment and under conditions of extreme confinement, only the transition of the mobile phase is captured, i.e., the Arrhenius component which corresponds to the fastest timescale among the distribution of relaxation times in the bulk glass transition. In agreement with experiment [8,63] the heat capacity step during glass transition at stretched δ_g/confined situations, appears smaller in magnitude compared to the bulk and with a tendency to stabilize. The reduced heat capacity step originating by the immobilization of the bound layer could then be related to a smoother reduction of the total entropy, leading to a stable, static liquid path with Arrhenius characteristics.

In addition to the polymer/nanofiller interactions that have been reported to affect T_g and mechanical properties [1,2], another parameter, usually not explicitly taken into account, can be associated with the ability (or inability) of the filler particles to diffuse efficiently. This property is affected by both their size and their shape and determines not only the quality of dispersion but also the entropy of the nanocomposite system. In our simulation, the GO flakes possess dimensions comparable to the size of the macromolecules so that GO/PAA interdiffusion is possible within the examined time window at temperatures above T_g. This is not uncommon in simulated polymer nanocomposites [75], as it allows for a more efficient sampling of the composite's microstates within the available time window. Since, in our case, the nanoflakes of GO contribute to the entropy of the system, their difficulty to diffuse results in an increase in the observed T_g. On the other hand, in cases where the nanofillers do no diffuse, they practically do not participate in entropy changes. Frequently, composite materials are prepared experimentally not only by melt-mixing, but also via sol-gel, in situ polymerization, or solvent evaporation techniques [1,8,37,76]. The so-prepared polymer nanocomposites exhibit both non-Einstein-like decrease in viscosity and improved mechanical properties [27,35,62,63,77]. This behavior can be reproduced in the framework of the present work by varying parameter δ_g.

Moreover, another parameter that is related to the aforementioned phenomenon is the size of the CRRs compared to the interparticle distance. It is well established in the literature that the radial distribution function of glassy materials above T_g although it depicts a structure, it is not the distance of the first peak that increases with the decreasing temperature but the height [25,27]. The formation of many small (of minimum diameter $\sim 3R_g$) rearranging nanophases is entropically more favorable than the formation of fewer larger phases. So, we may conclude that it is the percentage of the high density areas (blue regions in Fig. 2) that changes during cooling and not the size of them, leading to a normal distribution at T_g (Fig. 3). The formation of CRRs with dimensions near the polymer's R_g is considered as a good approximation for macromolecules with sizes below the entanglement molecular weight [27]. In cases of higher MW we may assume that the same chain can participate in more than one CRRs, mimicking thus the transition from Rouse to reptation dynamics. The predictions of the proposed EoS-

based model for high MWs will be presented in a future work.

4. Conclusions

On an effort to describe polymer dynamics in a common framework, both, below and above T_g, we have introduced a new VFT-like equation that incorporates a new parameter (δ_g) which describes the extent of the super-Arrhenius region. This approach allowed a consistent description of the glass transition phenomenology in the pristine polymer and in the composite systems. In the super-Arrhenius region two components for the diffusion are distinguished. Based on an interpretation related to the formation of structural heterogeneities due to the entropic force for diffusion, the activation energy was described as a sigmoidal function of temperature. The size of these heterogeneities in the composite systems was found to be normally distributed at T_g. The SLG equation in which the aforementioned sigmoidal function was inserted, provided a sound description of the change in the specific volume above and below the glass transition temperature, as this was determined by fully atomistic computer simulations.

Addition of the GO nanoflakes in the PAA matrix imparted an increase in the glass transition temperature of the composites. Examination of the decorrelation times of the backbone C−C bonds (associated with the α-relaxation) of PAA, exhibited increasingly slower dynamics in the nanocomposite systems as the content in GO was augmented. In agreement with past simulation works in polymer nanocomposites, the mechanical properties were improved by the insertion of the GO nanofillers. Investigation of the behavior of the shear modulus for various values of the parameter δ_g at constant T_g, showed an enhancement in the mechanical properties of the nanocomposites just above the T_g, in agreement with relevant experiments in polymer nanocomposites [4,8,63].

According to the presented analysis, the extension of the super-Arrhenius region (here implemented through the parameter δ_g) should also be taken into account when dealing with the dynamic and mechanical properties in polymer nanocomposites, especially in cases where an Arrhenius behavior and a non-Einstein-like decrease in viscosity is observed.

Acknowledgements

This research did not receive any specific grant from funding agencies in the public, commercial, or not-for-profit sectors.

Appendix A. Supplementary data

Supplementary data associated with this article can be found, in the online version, at http://dx.doi.org/10.1016/j.mtcomm.2017.11.006.

References

[1] Y. Song, Q. Zheng, Concepts and conflicts in nanoparticles reinforcement to polymers beyond hydrodynamics, Prog. Mater. Sci. 84 (2016) 1–58, http://dx.doi.org/10.1016/j.pmatsci.2016.09.002.
[2] C.G. Reid, A.R. Greenberg, Influence of silica reinforcement upon the glass transition behavior of acrylic polymers, J. Appl. Polym. Sci. 39 (1990) 995–1014, http://dx.doi.org/10.1002/app.1990.070390417.
[3] X. Wang, D. Tan, Z. Chu, et al., Mechanical properties of polymer composites reinforced by functionalized graphene prepared via direct exfoliation of graphite flakes in styrene, RSC Adv. 6 (2016) 112486–112492, http://dx.doi.org/10.1039/C6RA24479C.
[4] S. Merabia, P. Sotta, D.R. Long, A microscopic model for the reinforcement and the nonlinear behavior of filled elastomers and thermoplastic elastomers (Payne and Mullins Effects), Macromolecules 41 (2008) 8252–8266, http://dx.doi.org/10.1021/ma8014728.
[5] X. Qin, W. Xia, R. Sinko, et al., Tuning glass transition in polymer nanocomposites with functionalized cellulose nanocrystals through nanoconfinement, Nano Lett. 15 (2015) 6738–6744, http://dx.doi.org/10.1021/acs.nanolett.5b02588.
[6] C. Zhang, Y. Guo, R.D. Priestley, Glass transition temperature of polymer nanoparticles under soft and hard confinement, Macromolecules 44 (2011) 4001–4006, http://dx.doi.org/10.1021/ma1026862.
[7] F.W. Starr, J.F. Douglas, D. Meng, et al., Bound layers cloak nanoparticles in strongly interacting polymer nanocomposites, ACS Nano 10 (2016) 10960–10965, http://dx.doi.org/10.1021/acsnano.6b05683.
[8] G. Kritikos, Transition of the bounded polymer layer to a rigid amorphous phase: a computational and DSC study, Polym. (U.K.) 55 (2014) 4658–4670, http://dx.doi.org/10.1016/j.polymer.2014.07.048.
[9] A.M.K. Esawi, M.M. Farag, Carbon nanotube reinforced composites: potential and current challenges, Mater. Des. 28 (2007) 2394–2401, http://dx.doi.org/10.1016/j.matdes.2006.09.022.
[10] R.J. Young, I.A. Kinloch, L. Gong, et al., The mechanics of graphene nanocomposites: a review, Compos. Sci. Technol. 72 (2012) 1459–1476, http://dx.doi.org/10.1016/j.compscitech.2012.05.005.
[11] J.-T. Chen, Y.-J. Fu, Q.-F. An, et al., Tuning nanostructure of graphene oxide/polyelectrolyte LbL assemblies by controlling pH of GO suspension to fabricate transparent and super gas barrier films, Nanoscale 5 (2013) 9081–9098, http://dx.doi.org/10.1039/c3nr02845c.
[12] V. Mittal (Ed.), Polymer-Graphene Nanocomposites, RSC, Publishing, Cambridge, 2012, , http://dx.doi.org/10.1039/9781849736794.
[13] P. Mukhopadhyay, R. Gupta (Eds.), Graphite, Graphene, and Their Polymer Nanocomposites, CRC Press, 2012, , http://dx.doi.org/10.1201/b13051.
[14] M.M. Hasani-Sadrabadi, N. Mokarram, M. Azami, et al., Preparation and characterization of nanocomposite polyelectrolyte membranes based on Nafion ionomer and nanocrystalline hydroxyapatite, Polym. (Guildf.) 52 (2011) 1286–1296, http://dx.doi.org/10.1016/j.polymer.2010.11.033.
[15] S. Mogurampelly, O. Borodin, V. Ganesan, Computer simulations of ion transport in polymer electrolyte membranes, Annu. Rev. Chem. Biomol. Eng. 7 (2016) 349–371, http://dx.doi.org/10.1146/annurev-chembioeng-080615-034655.
[16] G. Hazell, M. Hinojosa-Navarro, T.M. McCoy, et al., Responsive materials based on magnetic polyelectrolytes and graphene oxide for water clean-up, J. Colloid Interface Sci. 464 (2016) 285–290, http://dx.doi.org/10.1016/j.jcis.2015.11.029.
[17] J. Zheng, X. Ma, X. He, et al., Praparation, characterizations, and its potential applications of PANi/graphene oxide nanocomposite, Procedia Eng. 27 (2012) 1478–1487, http://dx.doi.org/10.1016/j.proeng.2011.12.611.
[18] D. Priftis, Polyelectrolyte-graphene nanocomposites for biosensing applications, Curr. Org. Chem. 19 (2015) 1819–1827.
[19] D.D. Kulkarni, I. Choi, S.S. Singamaneni, et al., Graphene oxide − polyelectrolyte nanomembranes, ACS Nano. 4 (2010) 4667–4676.
[20] P. Li, Y. Zheng, M. Li, et al., Enhanced toughness and glass transition temperature of epoxy nanocomposites filled with solvent-free liquid-like nanocrystal-functionalized graphene oxide, Mater. Des. 89 (2016) 653–659, http://dx.doi.org/10.1016/j.matdes.2015.09.155.
[21] M. Mahkam, A.A. Rafi, L. Faraji, et al., Preparation of poly (methacrylic acid)–Graphene oxide nanocomposite as a pH-Sensitive drug carrier through in-situ copolymerization of methacrylic acid with polymerizable graphene, polym. plast. technol, Polym. Plast. Technol. Eng. 54 (2014) 916–922, http://dx.doi.org/10.1080/03602559.2014.961081.
[22] K.K. Sadasivuni, D. Ponnamma, J. Kim, et al. (Eds.), Graphene-based Polymer Nanocomposites in Electronics, Springer, 2015, , http://dx.doi.org/10.1007/978-3-319-13875-6.
[23] Y. Gao, H.-L. Yip, K.-S. Chen, et al., Surface doping of conjugated polymers by graphene oxide and its application for organic electronic devices, Adv. Mater. 23 (2011) 1903–1908, http://dx.doi.org/10.1002/adma.201100065.
[24] S. Faghihi, A. Karimi, M. Jamadi, et al., Graphene oxide/poly(acrylic acid)/gelatin nanocomposite hydrogel: experimental and numerical validation of hyperelastic model, Mater. Sci. Eng. C 38 (2014) 299–305, http://dx.doi.org/10.1016/j.msec.2014.02.015.
[25] E.J. Donth, The Glass Transition Relaxation Dynamics in Liquids and Disordered Materials, Springer, Berlin Heidelberg, 2001, http://dx.doi.org/10.1007/978-3-662-04365-3.
[26] R.P. White, J.E.G. Lipson, Polymer free volume and its connection to the glass transition, Macromolecules 49 (2016) 3987–4007, http://dx.doi.org/10.1021/acs.macromol.6b00215.
[27] G. Kritikos, N. Vergadou, I.G. Economou, Molecular dynamics simulation of highly confined glassy ionic liquids, J. Phys. Chem. C 120 (2016) 1013–1024, http://dx.doi.org/10.1021/acs.jpcc.5b09947.
[28] H. Vogel, The temperature dependence law of the viscosity of fluids, Phys. Zeit. 22 (1921) 645–646.
[29] G. Tammann, W. Hesse, The dependancy of viscosity on temperature in hypothermic liquids, Z. Anorg. Allg. Chem. 156 (1926) 245–257.
[30] G.S. Fulcher, Analysis of recent measurments of the viscosity of glasses, J. Am. Ceram. Soc. 8 (1925) (2017) 339–355, http://dx.doi.org/10.1111/j.1151-2916.1925. tb16731. x.
[32] W. Kob, Computer simulations of supercooled liquids and glasses, J. Phys. Condens. Matter. 11 (1999) 85–115.
[33] P. Debenedetti, F. Stillinger, Supercooled liquids and the glass transition, Nature 410 (2001) 259–267, http://dx.doi.org/10.1038/35065704.
[34] G. Anagnostopoulos, C. Androulidakis, E.N. Koukaras, et al., Stress transfer mechanisms at the submicron level for graphene/polymer systems, ACS Appl. Mater. Interfaces 7 (2015) 4216–4223, http://dx.doi.org/10.1021/am508482n.
[35] M.E. Mackay, T.T. Dao, A. Tuteja, et al., Nanoscale effects leading to non-Einstein-like decrease in viscosity, Nat. Mater. 2 (2003) 762–766, http://dx.doi.org/10.1038/nmat999.
[36] C.-T. Lu, A. Weerasinghe, D. Maroudas, et al., A comparison of the elastic properties of graphene- and fullerene-Reinforced polymer composites: the role of filler morphology and size, Sci. Rep. 6 (2016) 31735, http://dx.doi.org/10.1038/srep31735.
[37] L. Shao, J. Li, Y. Guang, et al., PVA/polyethyleneimine-functionalized graphene

composites with optimized properties, Mater. Des. 99 (2016) 235–242, http://dx.doi.org/10.1016/j.matdes.2016.03.039.
[38] B. Vorselaars, A.V. Lyulin, K. Karatasos, et al., Non-Gaussian nature of glassy dynamics by cage to cage motion, Phys. Rev. E Stat. Nonlinear Soft Matter Phys. 75 (2007) 11504, http://dx.doi.org/10.1103/PhysRevE.75.011504.
[39] D. Hudzinskyy, A.V. Lyulin, A.R.C. Baljon, et al., Effects of strong confinement on the glass-transition temperature in simulated atactic polystyrene films, Macromolecules 44 (2011) 2299–2310, http://dx.doi.org/10.1021/ma102567s.
[40] M. Solar, K. Binder, W. Paul, Relaxation processes and glass transition of confined polymer melts: a molecular dynamics simulation of 1, 4-polybutadiene between graphite walls, J. Chem. Phys. 146 (2017), http://dx.doi.org/10.1063/1.4975390 (203308).
[41] M.M. Shokrieh, Z. Shokrieh, S.M. Hashemianzadeh, A novel combined molecular dynamics-micromechanics method for modeling of stiffness of graphene/epoxy nanocomposites with randomly distributed graphene, Mater. Des. 64 (2014) 96–101, http://dx.doi.org/10.1016/j.matdes.2014.07.031.
[42] K.C. Daoulas, V.A. Harmandaris, V.G. Mavrantzas, Molecular dynamics simulation of a polymer Melt/Solid interface: local dynamics and chain mobility in a thin film of polyethylene melt adsorbed on graphite, Macromolecules 38 (2005) 5796–5809, http://dx.doi.org/10.1021/ma050176r.
[43] P.G. de Gennes, Glass transitions in thin polymer films, Eur. Phys. J. E. 2 (2000) 201–205, http://dx.doi.org/10.1007/pl00013665.
[44] K. Karatasos, G. Kritikos, Characterization of a graphene Oxide/Poly(acrylic acid) nanocomposite by means of molecular dynamics simulations, RSC Adv. 6 (2016) 109267–109277, http://dx.doi.org/10.1039/C6RA22951D.
[45] A.A. Chialvo, J.M. Simonson, Molecular dynamics simulation of the interfacial behavior of short-Chain polystyrene sulfonate aqueous solutions in contact with graphene surfaces in the presence of multivalent cations, J. Phys. Chem. C 112 (2008) 19521–19529, http://dx.doi.org/10.1021/jp8041846.
[46] J. Chen, L. Chen, Y. Wang, et al., Molecular dynamics simulations of the adsorption of DNA segments onto graphene oxide, J. Phys. D. Appl. Phys. 47 (2014) 505401, http://dx.doi.org/10.1088/0022-3727/47/50/505401.
[47] M. Azimi, S.S. Mirjavadi, A.M.S. Hamouda, et al., Heterogeneities in polymer structural and dynamic properties in graphene and graphene oxide nanocomposites: molecular dynamics simulations, Macromol. Theory Simul. 26 (2017) 1600086, http://dx.doi.org/10.1002/mats.201600086.
[48] W.D. Cornell, P. Cieplak, C.I. Bayly, et al., A second generation force field for the simulation of proteins, nucleic acids, and organic molecules, J. Am. Chem. Soc. 117 (1995) 5179–5197, http://dx.doi.org/10.1021/ja00124a002.
[49] J. Wang, W. Wang, P.A. Kollman, et al., Automatic atom type and bond type perception in molecular mechanical calculations, J. Mol. Graph. Model. 25 (2006) 247–260, http://dx.doi.org/10.1016/j.jmgm.2005.12.005.
[50] D. Stauffer, N. Dragneva, W.B. Floriano, et al., An atomic charge model for graphene oxide for exploring its bioadhesive properties in explicit water, J. Chem. Phys. 141 (2014) 44705, http://dx.doi.org/10.1063/1.4890503.
[51] L. Martinez, R. Andrade, E.G. Birgin, et al., PACKMOL: A package for building initial configurations for molecular dynamics simulations, J. Comput. Chem. 30 (2009) 2157–2164, http://dx.doi.org/10.1002/jcc.21224.
[52] R.E. Roussou, K. Karatasos, Graphene/poly(ethylene glycol) nanocomposites as studied by molecular dynamics simulations, Mater. Des. 97 (2016) 163–174, http://dx.doi.org/10.1016/j.matdes.2016.02.078.
[53] J.C. Phillips, R. Braun, W. Wang, et al., Scalable molecular dynamics with NAMD, J. Comput. Chem. 26 (2005) 1781–1802, http://dx.doi.org/10.1002/jcc.20289.
[54] S. Plimpton, Fast parallel algorithms for short-Range molecular dynamics, J. Comput. Phys. 117 (1995) 1–19, http://dx.doi.org/10.1006/jcph.1995.1039.
[55] I.C. Sanchez, R.H. Lacombe, An elementary molecular theory of classical fluids, Pure fluids, J. Phys. Chem. 80 (1976) 2352–2362, http://dx.doi.org/10.1021/j100562a008.
[56] R.P. White, J.E.G. Lipson, Thermodynamic treatment of polymer thin-film glasses, Phys. Rev. E Stat. Nonlinear Soft Matter Phys. 84 (2011) 1–6, http://dx.doi.org/10.1103/PhysRevE.84.041801.
[57] P.J. Flory, Principles of Polymer Chemistry, Cornell University Press, Ithaca, NY, 1953, http://dx.doi.org/10.1021/ja01639a090.
[58] L. Shao, J.L. Lutkenhaus, Thermochemical properties of free-standing electrostatic layer-by-layer assemblies containing poly(allylamine hydrochloride) and poly(acrylic acid), Soft Matter. 6 (2010) 3363, http://dx.doi.org/10.1039/c0sm00082e.
[59] D. Frenkel, Order through entropy, Nat. Mater. 14 (2014) 9–12, http://dx.doi.org/10.1038/nmat4178.
[60] G. Adam, J.H. Gibbs, On the temperature dependence of cooperative relaxation properties in glass-Forming liquids, J. Chem. Phys. 43 (1965) 139–146, http://dx.doi.org/10.1063/1.1696442.
[61] G. Kritikos, A.F. Terzis, Theoretical study of polymer brushes by a new numerical mean field theory, Polym. (Guildf.) 48 (2007) 638–651, http://dx.doi.org/10.1016/j.polymer.2006.11.039.
[62] S.H. Anastasiadis, K. Karatasos, G. Vlachos, et al., Nanoscopic-confinement effects on local dynamics, Phys. Rev. Lett. 84 (2000) 915–928, http://dx.doi.org/10.1103/PhysRevLett.84.915.
[63] G.P. Baeza, C. Dessi, S. Costanzo, et al., Network dynamics in nanofilled polymers, Nat. Commun. 7 (2016) 11368, http://dx.doi.org/10.1038/ncomms11368.
[64] A. Huwe, F. Kremer, P. Behrens, et al., Molecular dynamics in confining space: from the single molecule to the liquid state, Phys. Rev. Lett. 82 (1999) 2338–2341, http://dx.doi.org/10.1103/PhysRevLett.82.2338.
[65] N. Hao, M. Böhning, A. Schönhals, Dielectric properties of nanocomposites based on polystyrene and polyhedral oligomeric phenethyl-silsesquioxanes, Macromolecules 40 (2007) 9672–9679, http://dx.doi.org/10.1021/ma071777g.
[66] V.M. Nazarychev, A.V. Lyulin, S.V. Larin, et al., Molecular dynamics simulations of uniaxial deformation of thermoplastic polyimides, Soft Matter 7 (2016) 3972–3981, http://dx.doi.org/10.1039/C6SM00230G.
[67] I.G. Mathioudakis, G.G. Vogiatzis, C. Tzoumanekas, et al., Multiscale simulations of PS–SiO_2 nanocomposites: from melt to glassy state, Soft Matter 12 (2016) 7585–7605, http://dx.doi.org/10.1039/C6SM01536 K.
[68] J.-L. Tsai, J.-F. Tu, Characterizing mechanical properties of graphite using molecular dynamics simulation, Mater. Des. 31 (2010) 194–199, http://dx.doi.org/10.1016/j.matdes.2009.06.032.
[69] L.E. Nielsen, R.F. Landel, Mechanical Properties of Polymers and Composites, CRC Press, 1994.
[70] D. Cangialosi, A. Alegria, J. Colmenero, Effect of nanostructure on the thermal glass transition and physical aging in polymer materials, Prog. Polym. Sci. 54-55 (2016) 128–147, http://dx.doi.org/10.1016/j.progpolymsci.2015.10.005.
[71] G. Kritikos, A. Sgouros, G.G. Vogiatzis, et al., Molecular dynamics study of polyethylene under extreme confinement, J. Phys. Conf. Ser. 738 (2016) 12012, http://dx.doi.org/10.1088/1742-6596/738/1/012012.
[72] M. Krutyeva, A. Wischnewski, M. Monkenbusch, et al., Effect of nanoconfinement on polymer dynamics: surface layers and interphases, Phys. Rev. Lett. 110 (2013) 1–5, http://dx.doi.org/10.1103/PhysRevLett.110.108303.
[73] R. Pelster, U. Simon, Nanodispersions of conducting particles: preparation, microstructure and dielectric properties, Colloid Polym, Sci 277 (1999) 2–14, http://dx.doi.org/10.1007/s003960050361.
[74] C.G. Robertson, M. Rackaitis, Further consideration of viscoelastic two glass transition behavior of nanoparticle-filled polymers, Macromolecules 44 (2011) 1177–1181, http://dx.doi.org/10.1021/ma102631h.
[75] A. Karatrantos, R.J. Composto, K.I. Winey, et al., Polymer and spherical nanoparticle diffusion in nanocomposites, J. Chem. Phys. 146 (2017) 203331, http://dx.doi.org/10.1063/1.4981258.
[76] D. Ratna, S. Divekar, A.B. Samui, et al., Poly(ethylene oxide)/clay nanocomposite: thermomechanical properties and morphology, Polym. (Guildf.) 47 (2006) 4068–4074, http://dx.doi.org/10.1016/j.polymer.2006.02.040.
[77] M. Alcoutlabi, G.B. McKenna, Effects of confinement on material behaviour at the nanometre size scale, J. Phys. Condens. Matter 17 (2005) R461–R524, http://dx.doi.org/10.1088/0953-8984/17/15/R01.